



Fractal dimensions and morphological characteristics of aggregates formed in different physico-chemical and mechanical flocculation environments

Léa Guerin, Christine Frances, Alain Liné, Carole Coufort-Saudejaud

► To cite this version:

Léa Guerin, Christine Frances, Alain Liné, Carole Coufort-Saudejaud. Fractal dimensions and morphological characteristics of aggregates formed in different physico-chemical and mechanical flocculation environments. *Colloids and Surfaces A: Physicochemical and Engineering Aspects*, 2019, 560, pp.213-222. 10.1016/j.colsurfa.2018.10.017 . hal-01924034

HAL Id: hal-01924034

<https://hal.science/hal-01924034>

Submitted on 15 Nov 2018

HAL is a multi-disciplinary open access archive for the deposit and dissemination of scientific research documents, whether they are published or not. The documents may come from teaching and research institutions in France or abroad, or from public or private research centers.

L'archive ouverte pluridisciplinaire **HAL**, est destinée au dépôt et à la diffusion de documents scientifiques de niveau recherche, publiés ou non, émanant des établissements d'enseignement et de recherche français ou étrangers, des laboratoires publics ou privés.






Open Archive Toulouse Archive Ouverte

OATAO is an open access repository that collects the work of Toulouse researchers and makes it freely available over the web where possible

This is an author's version published in: <http://oatao.univ-toulouse.fr/21055>

Official URL: <https://doi.org/10.1016/j.colsurfa.2018.10.017>

To cite this version:

Guerin, Lea  and Frances, Christine  and Liné, Alain and Coufort, Carole 
Fractal dimensions and morphological characteristics of aggregates formed in different physico-chemical and mechanical flocculation environments. (In Press: 2019) Colloids and Surfaces A: Physicochemical and Engineering Aspects, 560. 213-222. ISSN 0927-7757

Any correspondence concerning this service should be sent
to the repository administrator: tech-oatao@listes-diff.inp-toulouse.fr

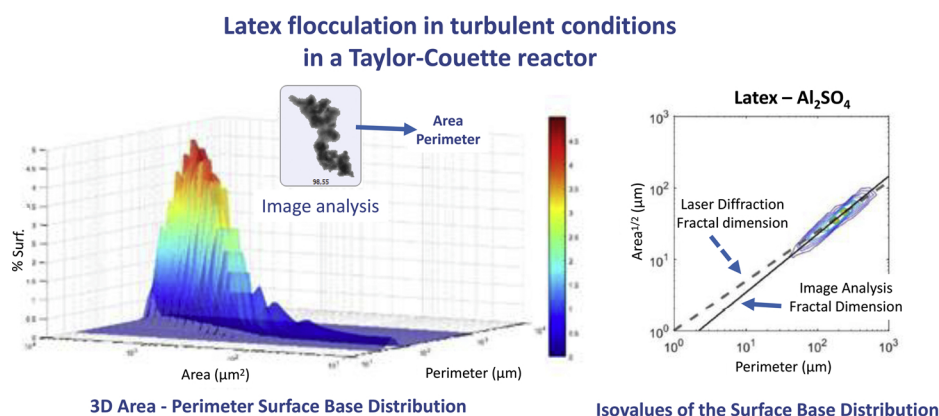
Fractal dimensions and morphological characteristics of aggregates formed in different physico-chemical and mechanical flocculation environments

Léa Guérin^a, Christine Frances^{a,*}, Alain Liné^b, Carole Coufort-Saudejaud^a

^a Laboratoire de Génie Chimique, Université de Toulouse, CNRS, Toulouse, France

^b LISBP, Université de Toulouse, CNRS, INRA, Toulouse, France

GRAPHICAL ABSTRACT



ABSTRACT

Flocculation experiments were performed in a Taylor-Couette reactor in turbulent conditions characterized by the mean shear rate. A sequenced hydrodynamic protocol was applied which consists in low and high shear rates steps allowing to promote respectively aggregation and breakage processes. The particle size distribution and the 3D fractal dimension were determined on line by laser diffraction while morphological parameters were characterized off line using an automated microscope coupled with image processing. After a first aggregation-breakage cycle, the flocs formed by charge neutralization have smaller sizes than during the first aggregation step when the main aggregation mechanism is the charge neutralization whereas coarser but more resistant aggregates can be produced by bridging mechanism. During the flocculation process, high shear rates calibrate the flocs, creating small flocs having a size close to the Kolmogorov microscale. These small flocs serve as bricks to form larger flocs when lower shear rates are applied and a full reproducibility is observed after one or two cycles of the sequence depending on the aggregation mechanism. A clear correspondence was put in evidence between the shear rate conditions and the volume base mean size or fractal dimension of flocs. The morphological fractal dimension, as well as the fractal dimension derived from laser measurements, are in good agreement with the mean trend of the morphological data but cannot represent the whole diversity of floc sizes and shapes. The 3D surface base area and perimeter distributions appear as a promising tool allowing a deeper analysis of the impact of physico-chemical and shear conditions on aggregate properties during a flocculation process.

1. Introduction

Morphological properties of particles, gathering size and shape characteristics are key properties in a large variety of industrial applications. For example, end-use properties of ceramics or pharmaceutical powders are usually linked to particle size and shape distributions. Likewise, in water production or waste water treatment, the physical properties of the suspended particles may impact the separation process efficiency. Indeed, robust and porous flocs are best required for a filtration process, while dense and compact flocs are preferred in decantation processes [1,2]. Just to remind the context, during a flocculation process, particles enter in contact thanks to diffusional forces induced by the brownian motion or hydrodynamic forces resulting from differential sedimentation or shear effects. After the collision, particles remain together or not, depending on their surface properties and on the medium properties. The aggregation may then result from charge neutralization if salts are used or sweep flocculation in presence of a precipitate or even bridging flocculation if a polymer having a long chain is adsorbed on two or more particles at the same time. Flocculation by depletion is another mechanism occurring in presence of a free polymer that forces the particles to adhere the ones to the others. Finally the aggregate will remain stable until the hydrodynamic forces are less important than the cohesion forces. So, during an aggregation process performed under fixed hydrodynamic and physico-chemical conditions, two steps are usually observed. Initially, an increase of the mean size is induced by the strong decrease of the number of suspending particles; the aggregation events being much more frequent than the breakage ones. The mean size stabilizes then due to the increase of the breakage events. During the second stage of the aggregation process, a stationary state is finally reached either once aggregation and breakage processes have stopped or due to the balance of the aggregation and breakage phenomena [3–6]. Higher the shear rate, more rapid is the growth of aggregates and their steady state mean size are lower [7,8]. Higher the shear rate, lower is also the distribution spread [9,10]. The aggregate mean size is then usually related in steady state conditions to the mean Kolmogorov microscale ($< \eta >$) or to the shear rate (G) on this form $d_{mean} \sim < \eta > \sim G^{-\gamma}$ where a value of 0.5 is often considered for γ [5,7,8,11–14]. More specifically, analyzing kaolin flocs generated by various mechanisms, Li et al. [15] showed that the stable floc size exponent γ varied between about 0.4 when flocs were obtained by a bridging mechanism to about 0.6 in the case of charge neutralization or sweep flocculation mechanisms.

Furthermore, the morphology or the compactness of the aggregates may be evaluated by the fractal dimension. Such a property may be of prime importance in some industrial applications such as water treatment since the floc settling velocities varie with the fractal dimension distribution [16]. Several authors reported that high shear rate conditions lead to more dense flocs having higher fractal dimensions [17–19]. Some authors [7,20] have introduced two fractal dimensions to characterize the whole population of aggregates, one fractal dimension for the smallest entities and the second one, higher than the previous one, for the largest aggregates. To explain this result, it is claimed that the large aggregates, which are more subjected to breakage processes, lose their more fragile parts. So after several successive events during a flocculation process, they become more and more dense and their fractal dimension increases. However, opposite results were recently reported by Moruzzi et al. [21] considering only aggregates of large sizes. They observed that higher fractal dimensions were obtained for lower shear rates and concluded that the behaviour of the aggregate structure was dependant on the predominance of the aggregation mechanisms, either cluster-cluster or particle-cluster in relation with shear conditions. In the same vein, analyzing the particle size and their number and two fractal dimensions, based one on a characteristic size and the other one on the perimeter, several authors [7,20,22] isolated the main mechanism involved among erosion,

breakage and restructuring and concluded on the impact on the aggregate structure.

Furthermore, to analyze the effect of hydrodynamic conditions on aggregate properties, a sequenced protocol varying the shear rate level may be performed allowing analyzing the reversibility of the flocculation process. Applying again the same shear rate after a first aggregation/breakage cycle, Kusters [23] observed that the mean size of latex particles in presence of salt was reversible. However, after this pioneer work, several authors [18,24–27] reported the irreversible nature of the flocculation process. Thus, the aggregate size after a re-aggregation step is almost systematically lower than after the first aggregation step. The reversibility of floc break-up process also depends on the flocculation mechanism. Concerning the flocculation of kaolin clay, Yukselen and Gregory [28] reported a significant irreversibility after the breakage step in presence of salts whereas using cationic polyelectrolytes, an almost complete recovery was observed during the re-growth step. Floc structure and strength are also influenced by floc history. For instance, a gradual shear increase allows obtaining flocs having a higher fractal dimension than those produced under stable conditions when one cycle of growth-breakage-growth is applied [29]. But, in real conditions, as in stirred vessels, aggregates are submitted to multiple steps of breakage-regrowth due to the heterogeneous nature of the hydrodynamics. So, even if many works were performed on the impact of the hydrodynamic conditions on the aggregate properties, the relationship between the hydrodynamic shear conditions, in particular in turbulent conditions, the aggregate morphology and the physico-chemical conditions, which control the aggregation mechanism, is not fully clear.

The aim of this work is to analyze the combined effect of physico-chemical and hydrodynamical turbulent conditions on floc properties. So the impact of different coagulation mechanisms, in particular charge neutralization and bridging flocculation, on the floc properties was investigated performing sequenced hydrodynamic flocculation experiments inside a Taylor-Couette reactor. The floc size distribution and the fractal dimension were measured on line by laser diffraction while shape distributions were obtained thanks to an image analysis treatment analyzing a great number of flocs at each sampling done over the experiments. Thus, it was possible to get reliable statistical data on both size and shape properties of flocs, as well as on their fractal dimension using different complementary methods. Finally, 3D area-perimeter distributions accounting simultaneously for both size and shape characteristics were derived. A special attention was paid on the effect of the aggregation mechanism on the morphological changes and the analysis of their reproducibility after multiple steps of breakage-regrowth under turbulent shear conditions. In complement a focus was made on the comparison of the fractal dimension deduced from laser sizer and the morphological properties of flocs based on their area and perimeter distributions.

2. Materials and methods

Latex microspheres with a diameter about 0.2 μm commercialised by Polysciences Inc as a suspension with a solid fraction of 2.5% have been used during all the experiments presented in this article. The volume size distribution determined by laser diffraction is unimodal with sizes ranging from 0.05 to 0.5 μm . The mean volume equivalent diameter is equal to 0.18 μm and the median to 0.16 μm . The chosen dimensions of the particles (with a diameter of less than 1 μm) permit to obtain a suspension which is representative of colloidal suspensions found in many applications.

Those latex microspheres have a high concentration of sulfates groups on their surfaces. The zeta potential is equal to -54 mV ($\pm 3 \text{ mV}$) at a temperature of 25 $^{\circ}\text{C}$, suggesting that the latex suspension was rather stable in these conditions. All the experiments presented below have been conducted at room temperature between 20 and 25 $^{\circ}\text{C}$ with a volume fraction of primary particles of 3.5×10^{-5} in demineralized water.

2.1. Coagulant properties

Several types of coagulants: sodium chloride, aluminium sulfate and a cationic polymer, were used during the experiments in order to investigate their impact on the properties of the latex aggregates. The properties of the coagulants and the methodology applied with each of them is detailed below :

- Sodium chloride NaCl: A salt solution was systematically prepared the day before the experiment with a NaCl concentration of 82 g/L, i.e. a molar concentration of 1.4 mol/L. With such a concentration, the density of the saline solution is close to the one of the primary particles (1055 kg m^{-3}) and permits to avoid settling phenomenon. Moreover, this concentration is sufficient to permit the destabilization of the latex suspension as it is higher than the critical coagulant concentration (ccc) which was found to be equal to 1.1 mol/L. Prior all the experiments, a saline solution degassing was done by placing the solution under high stirring during several hours, in order to avoid the apparition of bubbles during the measurements which could alter the results.
- Aluminum sulfate ($\text{Al}_2(\text{SO}_4)_3 \cdot 6\text{H}_2\text{O}$): This coagulant is frequently used in water treatment [30,31]. The aluminum sulfate concentration was settled in the reactor at a concentration of $5.4 \cdot 10^{-3} \text{ g/L}$ corresponding to a concentration in $[\text{Al}^{3+}]$ of $2 \cdot 10^{-4} \text{ mol/L}$ assuming that $[\text{Al}^{3+}]$ is the main species. Indeed, aluminum sulfate has several equilibria in solution as well as one precipitation equilibrium. Those equilibria have been described by Duan and Gregory [30]. The properties of the different species in the solution highly depend on the pH. It is thus important to note that the form of the aluminum in the solution will determine the aggregation mechanism that will occur between the particles. Indeed, depending on the solution pH and the aluminum concentration, several phenomenon can promote the particles aggregation. For low pH values (under 4.5) the main form of aluminum is Al^{3+} . It is a trivalent cation whom the positive charges will neutralize the negative charges that are at the latex particles surface and thus permit to the particles to enter in contact. For pH values higher than 5, a precipitate may appear: $\text{Al}(\text{OH})_3$, promoting aggregation by a sweep flocculation mechanism. In our study case, the pH is equal to 4.5. Charges neutralization is thus the main mechanism. The main species is here Al^{3+} with a smaller quantity of $\text{Al}(\text{OH})^{2+}$ and very few of $\text{Al}(\text{OH})_2^+$.
- A cationic polymer, polydiallyldimethylammonium chloride (PolyDADMAC) with a very high molecular weight (C595, Kemira) was used. PolyDADMAC is a liquid organic coagulant, frequently used in water treatment to permit the turbidity reduction [24]. It can be used jointly with other flocculants to reduce the water treatment costs. A small amount of long chain polymer added to a suspension permits the adsorption of the individual chains of the polymer simultaneously on several particles, thus allowing the bridging of those particles. This phenomenon is in general observed for a very precise dosage in polymer. Indeed, a too high or too low polymer concentration may limit the particles aggregation. In general, aggregates formed by bridging are more resistant to breakage than those created by salt addition. Preliminary experiments permitted to find the amount of polymer to add to promote the latex particles flocculation. Before each experiment, a 0.15 g/L polymer solution was prepared with demineralized water. Two liters of saline solution at 2 g/L were also prepared and 2 mL of the polymer solution were injected in it. Indeed, it has been observed that a small amount of salt was necessary to favor the adsorption of the polymer and the flocculation [32]. The polymer and salt solution was then placed under high stirring during several hours to permit the degassing of the solution.

2.2. Experimental devices and protocol

Flocculation experiments were conducted in a Taylor-Couette reactor. Details on this geometry may be found in Guerin et al. [33]. Sequenced hydrodynamic experiments were performed in turbulent conditions which will be characterized by the mean shear rate and the Kolmogorov microscale. They consist in alternatively low and high shear rate steps which mainly promote respectively aggregation and breakage mechanisms. The coagulation/flocculation step is a major process in several industrial applications as for example in drinking water treatment. This operation is usually done in stirred tanks in turbulent conditions. In such reactors, the hydrodynamics is highly heterogeneous so the flocs continuously pass from a zone where they are highly stressed to a zone where they are much less sheared. So repeated high and low shear rate steps allow miming real conditions occurring in stirred tanks working in turbulent conditions. Moreover, during the first moments of an aggregation process, the reproducibility of the experiments may be greatly affected by small changes in the initial conditions (modifying slightly the particle property distribution or delaying of a few moments the time when the coagulant is added or even changing the time needed for the coagulant injection ...). During a sequenced operation, after a first aggregation step, when a high shear rate is applied, the floc breakage gives birth to small aggregates that serve as bricks in the following aggregation step. So the reproducibility of the experiments is much better [14].

Each experiment started with a Low Shear Rate step (LSR) of a duration of 30 min followed by 5 steps of one hour each at alternatively High Shear Rate value (HSR) and LSR value. Each experiment is thus characterized by a LSR and a HSR value. During the runs, three LSR values were tested: 34, 65 and 112 s^{-1} , which represent three inner cylinder rotation speeds (18, 30 and 46 rpm). All the experiments were conducted applying the same high shear rate value (HSR) equal to 350 s^{-1} , which corresponds to a rotation speed of 111 rpm. In the following, the successive six steps will be named: A1, B1, A2, B2, A3, B3 in reference for A to an Aggregation step conducted at a low shear rate, and for B to a Breakage step performed applying a HSR value. The sequence will be illustrated in the Section 3.2.

The aggregation of latex particles was analyzed in line by laser diffraction (Malvern Instruments Mastersizer 2000) giving access to the particle size distribution and to the global fractal dimension. The fractal dimension (D_f) was directly deduced here from the negative slope of a log-log plot of the relative scattering intensity versus the modulus of the scattering wave vector. Indeed, under the assumption of no internal multiple scattering and due to the refractive (refractive index 1.58) and size (200 nm) properties of the latex primary particles, the Rayleigh-Debye-Gans approximation can be considered as valid [13,19,20,34]. The volume fractal dimension determined by this way lies between 1 for an aggregate constituted by primary particles stuck in a line and 3 for a well compacted spherical aggregate. This 3D-fractal dimension allows linking the aggregate mass or volume (V) to a characteristic size (L) on the following form:

$$V \propto L^{D_f} \quad (1)$$

Off line analysis was also performed using a microscope coupled with an image analysis treatment (Malvern Instruments Morphologi G3). About 100,000 floc images for each analyzed sample were captured and for each floc, basic data, such as the area or the perimeter, were determined. The Area (A) is the visual projected area of the particle measured in pixels and converted to microns. The Perimeter (P) is the total length of the object boundary, calculated by summing the length of the boundary pixels, and then converted to microns. Other morphological parameters (circularity, convexity, solidity, ...) can be derived from the area and perimeter of the actual floc and of its convex hull [33].

The results obtained from the image analysis treatment can also be used to get a morphological fractal dimension. The following

relationship between the area and the perimeter is often used [35]:

$$A \propto P_{pf}^{\frac{2}{D_{pf}}} \quad (2)$$

Using this definition, the morphological fractal dimension (D_{pf}) is equal to 1 for objects having a smooth contour and higher than 1 for an irregular contour. D_{pf} can easily be obtained from image analysis drawing the square root of the area versus the perimeter in a log scale. It may be noticed that flocs of a few pixels, i.e. those having a circle equivalent diameter smaller than 10 μm , were not taken into account in

the perimeter and D_{pf} calculations.

3. Results and discussion

3.1. Volume size distributions over the flocculation sequenced scheme

Whatever the chosen coagulant, the shear rate or the sequencing step, the stationary state was reached before the end of the step. Fig. 1 reports a comparison of the volume base particle size distributions, for the different coagulants at the end of the six steps for experiments

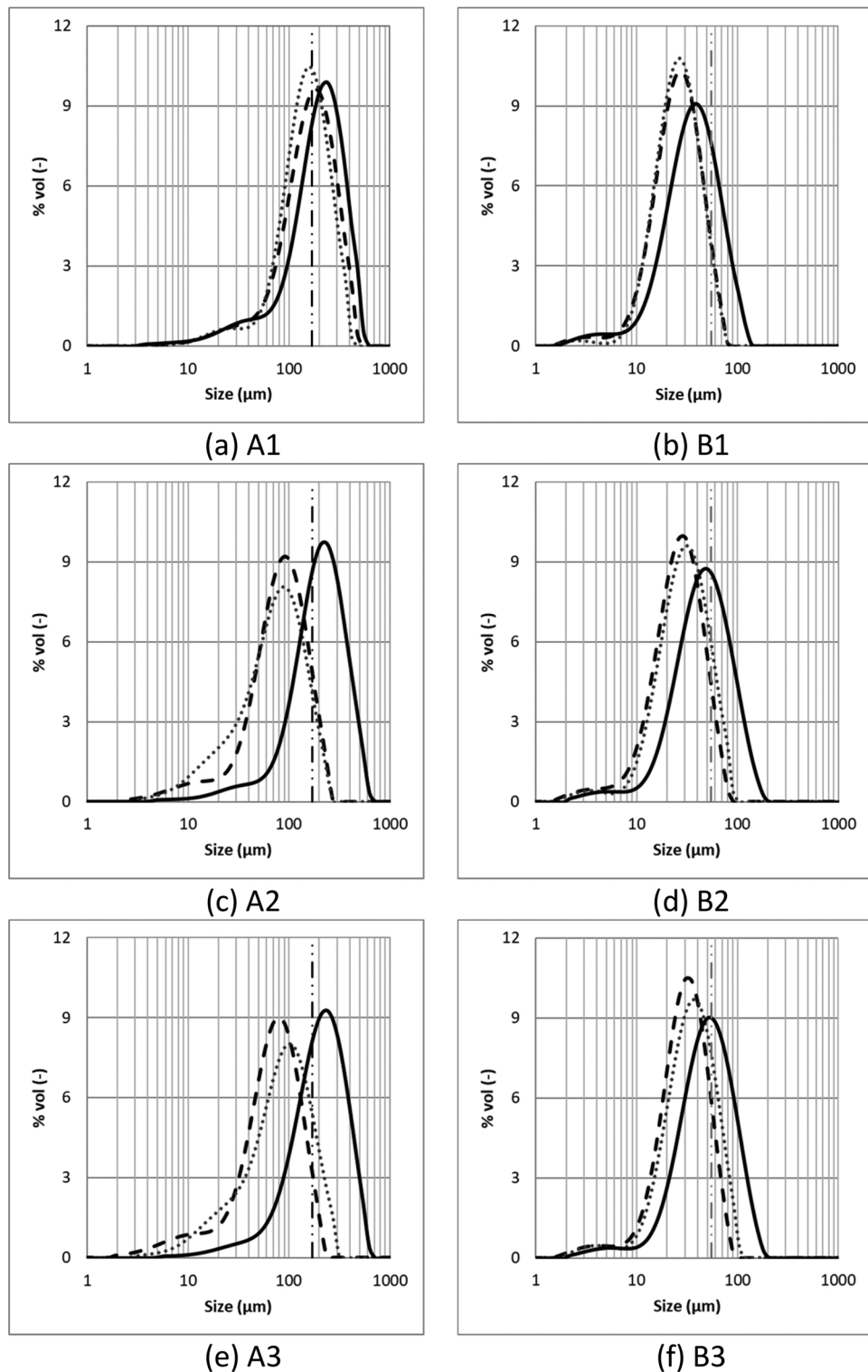


Fig. 1. Comparison of the volume size distribution of flocs obtained at the end of each hydrodynamic sequencing step for the three coagulants (LSR = 34 s⁻¹ and HSR = 350 s⁻¹).
—: Polymer —: NaCl: Al₂SO₄ —: $\eta_{LSR=34s^{-1}}$ —: $\eta_{HSR=350s^{-1}}$

conducted with LSR and HSR values respectively of 34 s^{-1} and 350 s^{-1} . On these graphs, vertical lines represent the mean values of the Kolmogorov microscale ($<\eta>$) calculated on the base of the mean shear rate applied ($<\eta> = 55 \mu\text{m}$ for $\text{HSR} = 350 \text{ s}^{-1}$ and $<\eta> = 170 \mu\text{m}$ for $\text{LSR} = 34 \text{ s}^{-1}$).

Whatever the hydrodynamic step, Fig. 1 shows that the volume size distributions are monomodal with a trail on the left, emphasizing the presence of some small flocs. While the first step conducted at a LSR value of 34 s^{-1} gives, in the case of the use of sodium chloride or aluminum sulfate, volume size distributions whom the mode is close to the value of the mean Kolmogorov micro scale, the use of the polymer permits the growth of much bigger aggregates (cf. Fig. 1a). The following step (cf. Fig. 1b), performed under HSR value induces the breakage of aggregates, whatever the type of coagulant. The modes of the volume size distributions are then all inferior to the mean Kolmogorov microscale value but the aggregates formed using the polymer appear to be bigger than those formed by charge neutralization. Whatever the mechanism, the increase of the shear rate leads to the appearance of small aggregates (whom the size ranges between $2\text{--}10 \mu\text{m}$). Even though the proportion of those small aggregates in the volume base distributions is low, their proportion would not be negligible looking at a number base distribution.

During the third step of the sequenced hydrodynamic experiments, at a LSR value of 34 s^{-1} (A2 – Fig. 1c), the volume size distributions obtained at stationary state reveal two different behaviors. When the aggregation mechanism is the charge neutralization, the flocs are smaller than those observed at the end of step A1 (Fig. 1a) with a mode lower than the value of the mean Kolmogorov microscale. Moreover, a substantial number of aggregates with a size of a few micrometers is remaining. Those small aggregates probably find their origin in the production of very small flocs during the previous step B1 (Fig. 1b). These small entities did not manage to aggregate during the following step. On the opposite, when the main mechanism is the bridging flocculation in presence of polymer, the mode of the distribution is higher than the mean Kolmogorov microscale value. Otherwise, the volume size distributions obtained after step 1 (A1 – Fig. 1a) and step 3 (A2 – Fig. 1c) seem similar, as if the aggregates were able to reconstruct identically. Furthermore, at the end of step 3 (A2 – Fig. 1c), almost all the smallest aggregates (whom the size ranges from 2 to $10 \mu\text{m}$) formed during the previous breaking step have disappeared.

During the following breakage steps (B2 – Fig. 1d and B3 – Fig. 1f), the volume size distributions obtained with sodium chloride are very close to those obtained at the end of step 2 (B1 – Fig. 1b). It seems that the flocs population did not change during those breakage steps, which suggests that a floculi population was created during step 2 (B1) and that those floculi are regenerated during each breakage step. The

volume size distribution obtained at the end of the last step at LSR value (A3 – Fig. 1e) is similar to the one obtained at the end of step 3 (A2 – Fig. 1c). For the runs performed using aluminum sulfate or polymer, the aggregates formed after steps B2 (cf. Fig. 1d) and B3 (cf. Fig. 1f) are bigger than those obtained with sodium chloride. Unlike the case with sodium chloride, the volume size distributions also slightly evolve from one breakage step to the other in the case of the use of aluminum sulfate or the polymer. However, the distributions obtained with the polymer are much more shifted to the right than those obtained with aluminum sulfate or sodium chloride. This increase is even so important using the polymer that the mode of the distribution after step B3 (Fig. 1f) has the same value than the mean value of the Kolmogorov microscale ($55 \mu\text{m}$ in that case). That points out the ability to produce larger aggregates by bridging flocculation. The successive steps of breakage and re flocculation permitted to produce in those hydrodynamic conditions aggregates that are more resistant although having larger sizes.

In order to better understand the evolution in size of the latex aggregates, a representation of the six volume size distributions obtained at steady state at the end of each step of the hydrodynamic sequence (for LSR and HSR values of respectively 34 and 350 s^{-1}) are represented for each of the three coagulants on Fig. 2. The two vertical lines represent, from left to right, the values of the mean Kolmogorov microscale at $\text{HSR} = 350 \text{ s}^{-1}$ ($<\eta> = 55 \mu\text{m}$) and $\text{LSR} = 34 \text{ s}^{-1}$ ($<\eta> = 170 \mu\text{m}$).

The distributions obtained with NaCl emphasize a strong decrease of the aggregates sizes between step 1 (A1) and 3 (A2), although conducted at the same LSR value. The mode obtained at the end A1 coincides with the mean value of the Kolmogorov microscale. The three distributions obtained after the three steps conducted at HSR value (B1, B2 and B3) highlight a strong decrease of the aggregates sizes with an increase of the shear rate. Otherwise, those three distributions are nearly superimposed. Under such hydrodynamic and physico-chemical conditions, the volume size distributions at the beginning of a step do not seem to influence the distributions obtained at the end of the steps conducted at HSR value ($\text{HSR} = 350 \text{ s}^{-1}$). Similar ascertainment can be made concerning the results obtained under similar conditions with aluminum sulfate. As for the distributions obtained with the use of a polymer (polyDADMAC), they are characterized by the presence of two modes: one for distributions obtained at the end of steps conducted at LSR values and the other one obtained at the end of steps conducted at HSR values. The distribution at the end of a low shear rate step thus also appears to be independent of the initial distribution.

Other runs were performed changing the LSR values ($\text{LSR} = 65 \text{ s}^{-1}$ or $\text{LSR} = 112 \text{ s}^{-1}$) while the HSR was always kept constant at 350 s^{-1} . Whatever the coagulant, higher is the shear rate, lower are the aggregate sizes. When sodium chloride or aluminium sulfate are used, the mode of

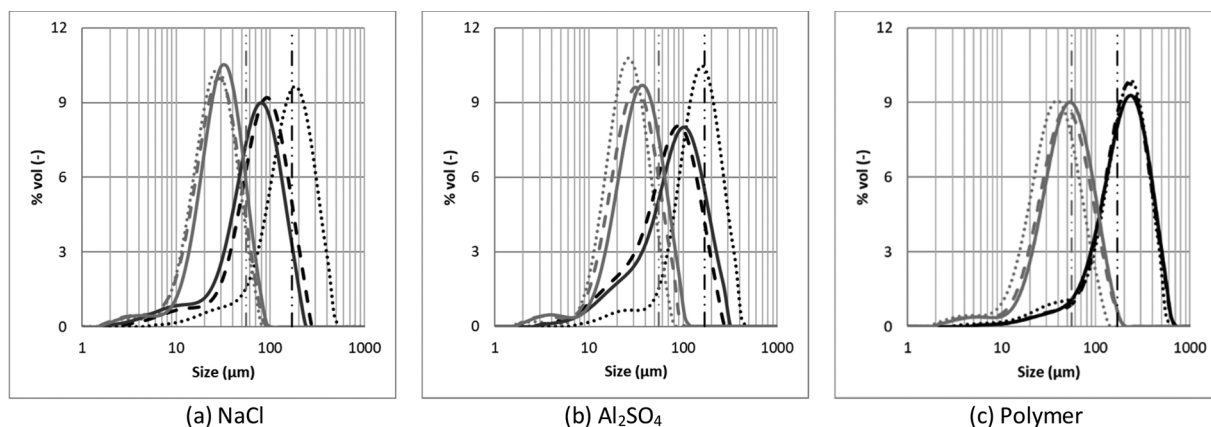


Fig. 2. Volume size distributions of latex aggregates at the end of each sequencing step ($\text{LSR} = 34 \text{ s}^{-1}$ and $\text{HSR} = 350 \text{ s}^{-1}$) for the three coagulants.

.....: A1 —: A2 —: A3 —: $\eta_{\text{LSR}=34\text{s}^{-1}}$
: B1 —: B2 —: B3 —: $\eta_{\text{HSR}=350\text{s}^{-1}}$

the volume base size distributions is lower than the Kolmogorov microscale after the first sequence step. In presence of the polymer, applying low LSR values, it is possible to create aggregates larger than the mean Kolmogorov microscale. It seems that the flocs formed in these hydrodynamic constraints have such a cohesion force that they cannot be broken compared to aggregates formed by charge neutralization. However, when the LSR value is increased ($LSR = 65 \text{ s}^{-1}$) in presence of the polymer, the hydrodynamic constraints are a drag on the formation of aggregates. Increasing again the LSR value ($LSR = 112 \text{ s}^{-1}$) the formation of aggregates was extremely difficult and had a poor reproducibility. Moreover, the use of aluminium sulfate always allows obtaining slightly larger aggregates than using sodium chloride and the higher is the preceding LSR value, the higher is the aggregate size formed applying a HSR value. So, even if the same mechanism acts in presence of sodium chloride or aluminium sulfate, the effect of hydrodynamics on the aggregate size is not exactly the same. These results put in evidence a combined effect of hydrodynamics and physico-chemical conditions on the aggregate properties.

3.2. 3D fractal dimension of latex floc

Particle size analysis data were used to evaluate the 3D fractal dimension of latex flocs for the different runs presented before changing the physico-chemical and/or hydrodynamic conditions. The evolution of the fractal dimension value obtained in presence of aluminum sulfate for each of the three tested LSR values is presented on the lower part of Fig. 3. The corresponding evolution of the volume-moment mean size X

(4,3) is also reported (intermediate section of Fig. 3) as well as a scheme of the hydrodynamic sequencing experiment on the top part of Fig. 3 allowing pointing out the correspondence between the changes of the shear rate and the characteristic size and fractal dimension of flocs.

At the beginning of the flocculation process, only primary particles are in suspension. Those particles quickly create small flocs constituted of a few primary particles, not large enough to be considered as fractal objects. Indeed, many authors such as Adachi et al. [36], and Takayasu and Galembeck [37] agree that the fractal dimension can only have a physical meaning if a minimum number of primary particles form the aggregate. Depending on authors, this number is estimated between 5 and 16. The observation of the evolution of the volume size distribution across time shows that the primary particles population is only preponderant during the first moments, then, the aggregates population becomes the major one. Thus, the fractal dimension data are only provided after a sufficiently long time in order to be able to consider that the aggregates structure is fractal. The more the shear rate during step 1 (A1) is low, the more the needed time to obtain an aggregates population for which the determination of a fractal dimension has a meaning is long (about 7 min at $LSR = 34 \text{ s}^{-1}$, about 5 min at $LSR = 65 \text{ s}^{-1}$ or 112 s^{-1}). In theory, this 3D fractal dimension ranges between 1 for linear objects to 3 for spherical ones. Note that the scale of the Fig. 3 was expanded to better show the changes in the fractal dimension value.

During step 1 (A1), the fractal dimension value regularly increases while the mean size reaches a stationary level much sooner. At the end of this step, for LSR values of 34 s^{-1} , the fractal dimension is about

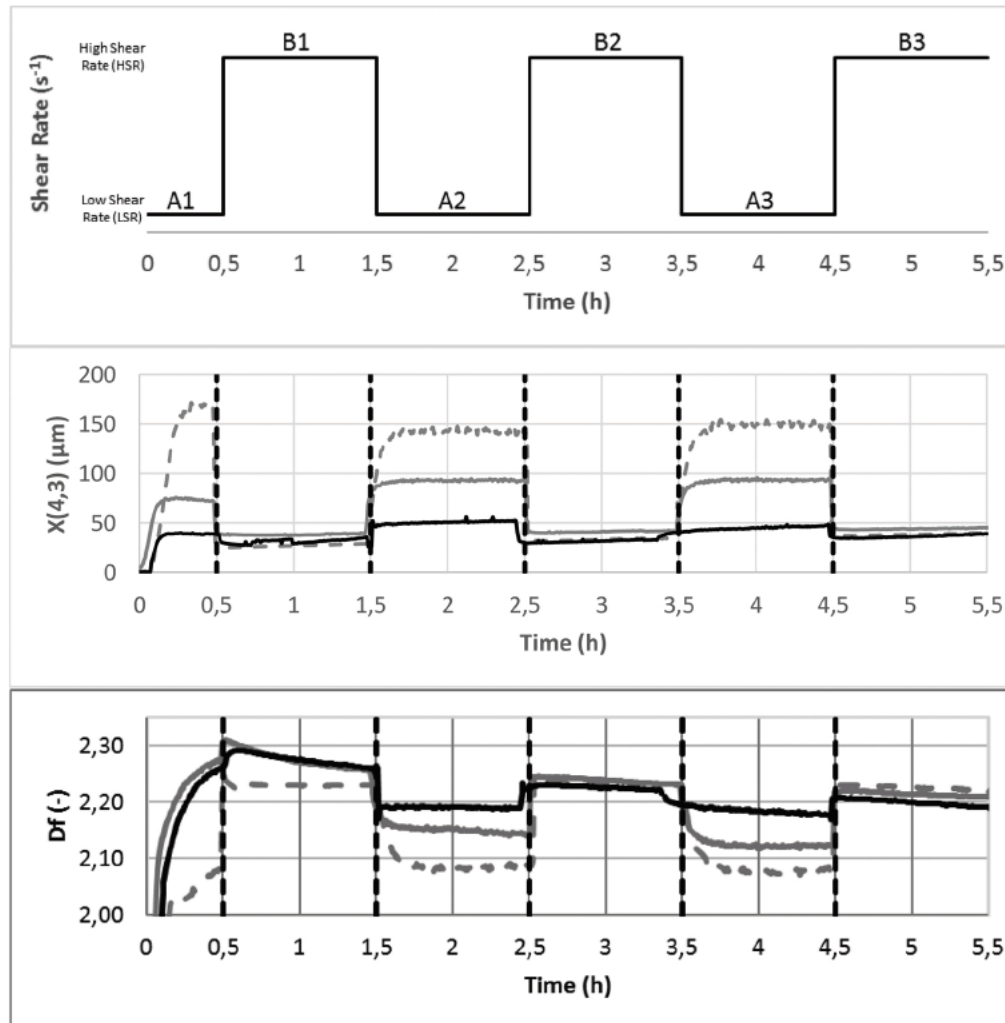


Fig. 3. $X(4,3)$ and fractal dimension evolutions across the hydrodynamic sequencing scheme in presence of aluminum sulfate at three LSR values: 34, 65 and 112 s^{-1} .
 - - - : $LSR = 34 \text{ s}^{-1}$ — : $LSR = 65 \text{ s}^{-1}$ — : $LSR = 112 \text{ s}^{-1}$

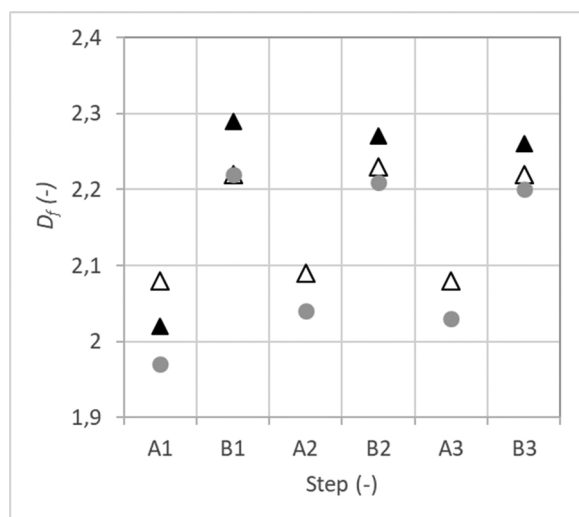


Fig. 4. Comparison of the steady fractal dimensions at the end of each step of the hydrodynamic sequencing scheme for $LSR = 34 \text{ s}^{-1}$ and $HSR = 350 \text{ s}^{-1}$ for the three coagulants.

▲: NaCl △: Al₂SO₄ •: Polymer

2.08. When the LSR values are 65 and 112 s^{-1} , it ranges between 2.25 and 2.3. Those orders of magnitude are coherent with those found in the literature [7,20,38,39]. Thereafter, whatever the experiment under consideration, the change in the shear rate value is easily identifiable on the fractal dimension graph. Indeed, the fractal dimension value is higher during HSR steps than LSR steps. As it has been pointed out by several authors [7,20,38], a correlation between the fractal dimension values and the hydrodynamic conditions in the reactor can be drawn. Aggregates submitted to strong hydrodynamic constraints are significantly denser and more compact and thus have higher fractal dimension values, closer to the sphere one. Thus, on Fig. 3, an increase in the fractal dimension value is visible during the first moments of the breaking step during which the flocs size decreases. Indeed, during the first minutes at HSR value, the aggregates formed during the breakage steps are more compact, denser and the fractal dimension grows slightly. However, the fractal dimension value thereafter continuously decreases during the breakage steps (steps B1, B2 and B3) which suggests that the aggregates are becoming less and less compact or that their surfaces become rougher. Moreover, the fractal dimension value at the end of a HSR step appears to be little dependent on the initial structure of the aggregates. Indeed, whatever the fractal dimension at the end of steps A1, A2 and A3, the fractal dimension value obtained at the end of the HSR steps remains the same. From one step to the other, it is possible to notice that the fractal dimension during the breakage steps slightly decreases. Fractal dimension values decrease from 2.25 to 2.2 between step 2 (B1) and step 6 (B3). In order to interpret those results, it is necessary to take a joint interest in the evolution across time of the aggregates sizes. It can be noticed on Fig. 3 that when the shear rate is turned on HSR value (at the beginning of steps B1, B2 or B3), the mean size suddenly drops. During these steps, the observation of the graphs does not permit to show a clear evolution in the $X(4,3)$ values but a deeper examination reveals a slight increase in the $X(4,3)$ value during all the breakage steps (steps B1, B2 and B3). For example, in the case of an experiment conducted under a LSR value of 112 s^{-1} , the $X(4,3)$ increases from 37 to $40 \mu\text{m}$ during step B1. Thus, even if during such a step, breakage phenomenon are predominant, some aggregation events can also occur. Given the very low increase in size, it can be thought that those aggregation phenomenon probably occur between a floculi generated at the beginning of the breakage step and very small aggregates (with a diameter of only a few micrometers) which will thus have a minor impact on the volume size distribution and the mean aggregates size.

Concerning the aggregation steps A2 and A3, the fractal dimension value is even lower when the low shear rate value is low. This result is again in coherence with the literature results indicating that the more the hydrodynamic constraints are high, the more the aggregates are compact and thus have a high fractal dimension. A decrease in the D_f values is also visible from one LSR step to the other (A1, A2 and A3). If such a decrease in the fractal dimension value is logically accompanied by a significant increase of the $X(4,3)$ as between steps A2 and A3 conducted at a LSR value of 34 s^{-1} , this observation cannot always be made between steps A1 and A2 of the same experiment. The correlation between the aggregates mean size and structure is more complex than it seems. It is necessary to remain cautious concerning the evolution of the fractal dimension value during a step or between different steps conducted at a same shear rate value since the changes are very small and it is thus difficult to evaluate the accuracy of the fractal dimension values obtained by laser diffraction.

Furthermore, the above data corresponding to values obtained in steady-state conditions at the end of the aggregation (A3) and breakage events (B3) in presence of aluminium sulfate follow a power law between the particle size $X(4,3)$ and the shear rate G . The power law coefficient is equal to 0.51 in good agreement with the data reported in the literature [5,7,8,11–14], also putting in evidence the good relationship between the mean size and the Kolmogorov microscale.

The same analysis was made with the other coagulants and the fractal dimensions obtained at the end of each step in the case where $LSR = 34 \text{ s}^{-1}$ and $HSR = 350 \text{ s}^{-1}$ for the three coagulants are compared on Fig. 4. Fig. 4 clearly puts in evidence the shift of the fractal dimensions from low values when a LSR value is applied to higher values corresponding to HSR steps. This first result may be directly correlated with the floc size. Larger are the flocs, less compact or spherical they are. Moreover, whatever the step, lowest fractal dimensions are obtained for the runs performed in presence of polymer, for which the largest aggregates were also observed as seen before. These coarse aggregates are thus less dense and compact than those formed by charge neutralization. This observation may be related to the bridging flocculation mechanism leading to the formation of poorly dense flocs as reported by Gregory [40]. The comparison of the fractal dimensions for the flocs produced by the two coagulants mainly acting by charge neutralization reveals higher values during HSR steps when sodium chloride is used, while smaller aggregates were observed (see the right column on Fig. 1). This behaviour may again simply reflects a size effect. Finally, if we compare the fractal dimensions for these two coagulants during LSR steps, a higher value is obtained for aluminium sulfate for the first aggregation step (A1) coinciding as expected with slightly smaller aggregates (Fig. 1a). However rather similar values of the fractal dimensions for both coagulants are get for the next two aggregation steps (A2) and (A3) whereas significantly different size distributions were observed (Fig. 1c and e). In that case, the fractal dimension of those rather disperse or even multimodal populations of flocs probably introduce compensating effect. Again, the sensitivity of the fractal dimension and its complex link with the size characteristics of flocs may be put forward.

3.3. Morphological analysis of flocs based on area and perimeter

Let's consider now the morphological results obtained from image analysis. It is possible for each floc to determine its area and perimeter and then to get the area and perimeter distributions analysing the whole population of flocs. As an example, Fig. 5a and b report respectively the surface base area and perimeter distributions at steady-state at the end of each step of the hydrodynamic sequencing scheme in the case of aluminium sulfate. On these graphs, the area (or perimeter) are indicated on the x-axis in a logarithmic scale and on the y-axis is reported the surface fraction, which is the sum of the surfaces of all flocs whose the area (or perimeter) belongs to a specific class divided by the total area of flocs. The area and perimeter distributions are

monomodal and quite similar, although they do not have the same range on x-axis. The area distributions spread over more than two decades, approximately between 60 and 15,000 μm^2 and the perimeter distributions range between about 30 and 1000 μm . Some disparities on the graphs can be noticed, however two main groups of curves can be clearly detected on each of them. The first one correspond to the aggregation steps (A1, A2 and A3) for which the area and the perimeter are higher and the second group correspond to the breakage steps (B1, B2 and B3), characteristic of smaller flocs. As suspected looking at these graphs, the area, which is linked to the floc size, and the perimeter, which can be seen as a surface shape characteristic, are related the one to the other. An example of the raw data concerning the area and the perimeter of each floc for one sample is given (Fig. S1) in the Supplementary material. Increasing the floc size, both the perimeter and the area increase. However, for a given area (or for a given perimeter), disparities on the floc perimeter (respectively floc area) arise and the range of variation increases with the aggregate size.

To better highlight the relationship between the area and the perimeter distributions, the 3D-surface density as function of the floc area and perimeter has been considered. An example is given on Fig. S2 on Supplementary material for a sequenced run performed in presence of aluminium sulfate using $\text{LSR} = 34 \text{ s}^{-1}$ and $\text{HSR} = 350 \text{ s}^{-1}$. Fig. S2—a corresponds to a typical aggregation step (A3) and Fig. S2-b to a breakage one (B3). The projections of 3D-surface densities are reported on Fig. 6 in which the square root of the area is drawn versus the perimeter. Isovalues of the surface base distribution are presented for the run performed at $\text{LSR} = 34 \text{ s}^{-1}$ and $\text{HSR} = 350 \text{ s}^{-1}$ and corresponding to typical aggregation (A3) and breakage (B3) steps for each coagulant. Similar results were observed for the runs performed under different hydrodynamic conditions (see Fig. S3 on Supplementary materials). Considering the relationship between the area and perimeter according to Eq. (2), the alignment on the first bisector represents the inverse of the morphological fractal dimension $1/D_{pf}$. Whatever the physico-chemical and hydrodynamical conditions, $1/D_{pf}$ seems to represent quite well the mean trend of the cloud resulting from morphological analysis. Moreover, the 3D fractal dimension obtained from laser diffraction measurements has been converted into a 2D fractal dimension, taking $D_f/3$, and also reported on these graphs (dotted line). To help comparing this fractal dimension to the plot slope and to the inverse of the morphological fractal dimension, the dotted line passes by the distribution mode. Whatever the step of the hydrodynamic sequencing step and the type of coagulant, a better agreement between the fractal dimension deduced from diffraction measurement and the

slope of the cloud is observed for the upper part of the scatter graph corresponding to the largest aggregates. This result is not surprising since the fractal dimension deduced from laser diffraction is on a volume base and thus it could be more representative of the largest entities. It is also obvious from these graphs that the fractal dimension, whether the volume-based fractal dimension or the morphological one, only gives a mean trend, and it is not able to represent the whole diversity of flocs shape.

Graphs such as the ones reported on Fig. 6 contain all the needed data to model a flocculation process in which both size and shape of aggregates should be tracked. Indeed, these data could be integrated into a population balance model tracking the two basic information; i.e. the floc area and perimeter since from these two basic parameters, other morphological descriptors such as the CED or the circularity could be deduced.

4. Conclusion

A sequenced hydrodynamic protocol was used to analyze a latex flocculation process in turbulent conditions in a Taylor-Couette reactor. The combined effects of physico-chemical and hydrodynamic conditions on floc size and shape properties were examined using three types of coagulants mainly acting by charge neutralization for two of them (sodium chloride and aluminum sulfate) and bridging flocculation for the last one (PolyDADMAC). The main following conclusions can be drawn:

- When the aggregation mechanism is the charge neutralization, the flocs obtained during a re-aggregation step are smaller than those formed during the first aggregation step and the mode of the volume size distribution is lower than the value of the mean Kolmogorov microscale. On the opposite, when the main mechanism is the bridging flocculation, the volume size distributions obtained during an aggregation or a re-aggregation step seem similar and aggregates larger than the mean Kolmogorov microscale can be formed. These results put in evidence the ability to produce larger aggregates in presence of a polymer. The successive steps of breakage and re flocculation permitted to produce aggregates that are more resistant by bridging flocculation although having larger sizes than by charge neutralization.
- A clear correspondence was put in evidence between the changes of the shear rate and the characteristic size or fractal dimension of flocs. Aggregates submitted to strong hydrodynamic constraints are

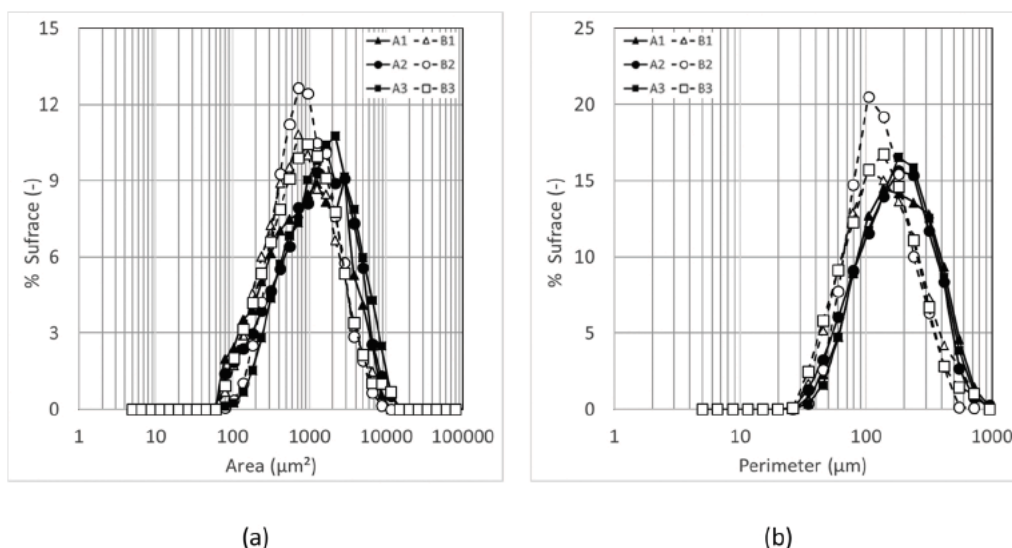


Fig. 5. Surface base distributions obtained at the end of each hydrodynamic sequencing step ($\text{LSR} = 34 \text{ s}^{-1}$ and $\text{HSR} = 350 \text{ s}^{-1}$) in presence of aluminum sulfate. a) area b) perimeter.

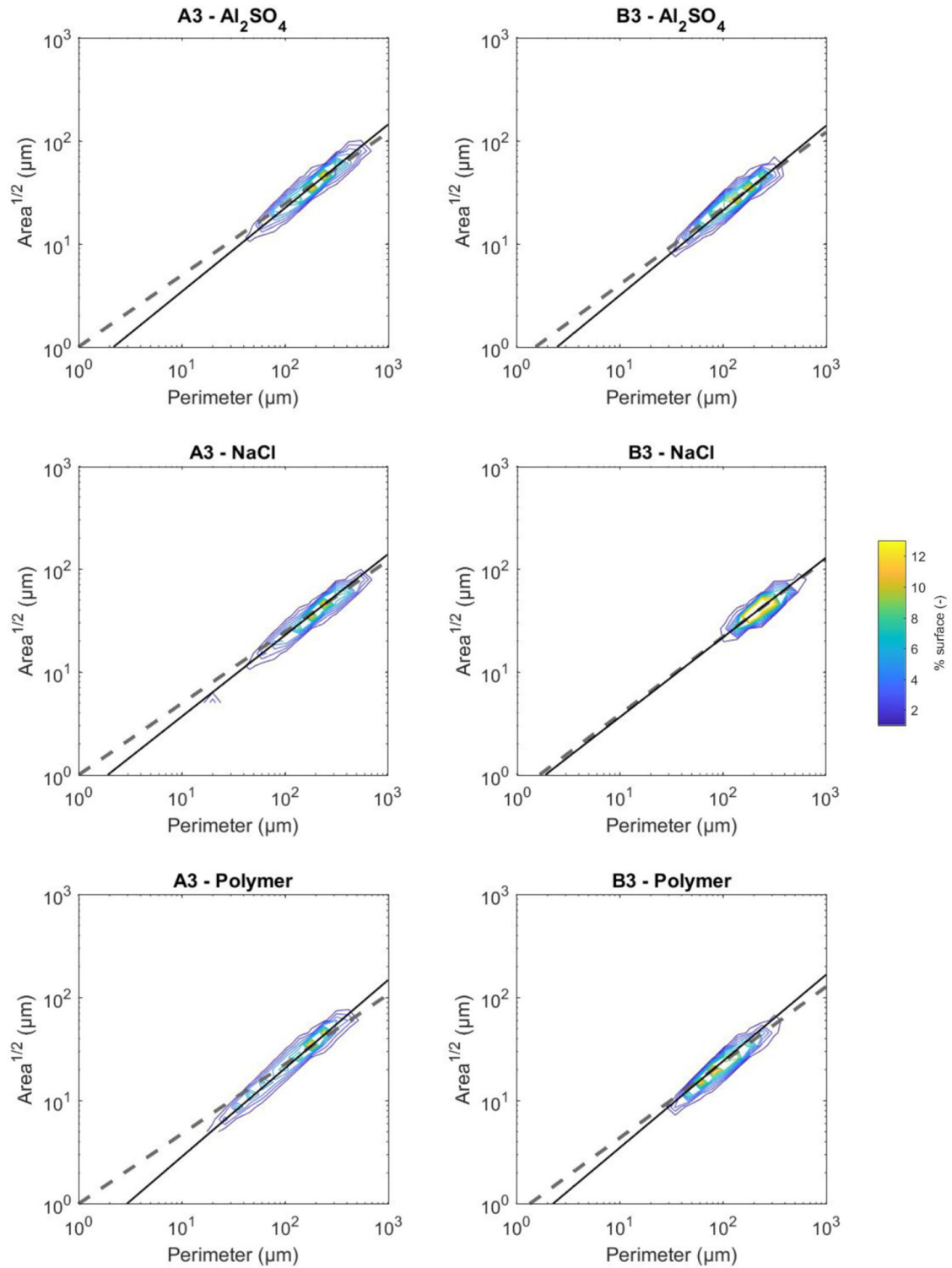


Fig. 6. Isovalues of the surface base distribution on a 2D graph drawing the square root of the area versus the perimeter – Data related to the run performed at $\text{LSR} = 34 \text{ s}^{-1}$ and $\text{HSR} = 350 \text{ s}^{-1}$ for the three coagulants for an aggregation step (A3) and a breakage step (B3).

—: Based on morphological fractal dimension ($1/D_{\text{pf}}$)
 - - -: Based on laser diffraction fractal dimension ($D_{\text{f}}/3$)

significantly denser and more compact and thus have higher fractal dimension values than those created under moderate shear conditions. Moreover, under similar hydrodynamic conditions, coarser aggregates, less dense and compact are obtained in presence of polymer compared to those formed by charge neutralization.

- The morphological fractal dimension deduced from the relationship

between the floc area and their perimeter represent quite well the mean trend of the statistical results but it is not able to represent the whole diversity of flocs shape. The fractal dimension derived from diffraction measurements is more representative of the mean trend of the largest aggregates.

- The area and perimeter surface base distributions revealed

similarities since both of them are related to the floc size. However, for a given area, strong disparities on perimeter may be observed and vice versa. So, 3D area-perimeter distributions allowing to analyse the change over the hydrodynamic conditions of the population of flocs appeared as an reliable tool to observe the impact of physico-chemical or hydrodynamical conditions on floc size and shape properties. The area and perimeter distributions obtained by image analysis could be integrated into a bidimensionnel population balance modelling in order to track both size and shape properties of aggregates over a flocculation process.

Appendix A. Supplementary data

Supplementary material related to this article can be found, in the online version, at doi:<https://doi.org/10.1016/j.colsurfa.2018.10.017>.

References

- [1] J. Nan, W. He, Characteristic analysis on morphological evolution of suspended particles in water during dynamic flocculation process, *Desalin. Water Treat.* 41 (1–3) (2012) 35–44, <https://doi.org/10.1080/19443994.2012.664676>.
- [2] M. Soos, A.S. Moussa, L. Ehrl, J. Sefcik, H. Wu, M. Morbidelli, Effect of shear rate on aggregate size and morphology investigated under turbulent conditions in stirred tank, *J. Colloid Interface Sci.* 319 (2) (2008) 577–589, <https://doi.org/10.1016/j.jcis.2007.12.005> ISSN 0021-9797.
- [3] P.T. Spicer, S.E. Pratsinis, M.D. Trennepohl, G.H.M. Meesters, Coagulation and fragmentation: the variation of shear rate and the time lag for attainment of steady state, *Ind. Eng. Chem. Res.* 35 (1996) 3074–3080, <https://doi.org/10.1021/ie950786n>.
- [4] T. Serra, X. Casamitjana, Effect of the shear and volume fraction on the aggregation and breakup of particles, *AIChE J.* 44 (8) (1998) 1724–1730, <https://doi.org/10.1002/aic.690440803> ISSN 1547-5905.
- [5] A. Biggs, P.A. Lant, Activated sludge flocculation: on-line determination of floc size and the effect of shear, *Water Res.* 34 (9) (2000) 2542–2550, [https://doi.org/10.1016/S0043-1354\(99\)00431-5](https://doi.org/10.1016/S0043-1354(99)00431-5) ISSN 0043-1354.
- [6] D. Bouyer, A. Liné, A. Cockx, Z. Do-Quang, Experimental analysis of floc size distribution and hydrodynamics in a jar-test, *Chem. Eng. Res. Des.* 79 (8) (2001) 1017–1024, <https://doi.org/10.1205/02638760152721587> ISSN 0263-8762.
- [7] V. Oles, Shear-induced aggregation and breakup of polystyrene latex particles, *J. Colloid Interface Sci.* 154 (1992) 351–358, [https://doi.org/10.1016/0021-9797\(92\)90149-G](https://doi.org/10.1016/0021-9797(92)90149-G).
- [8] T. Serra, J. Colomer, X. Casamitjana, Aggregation and breakup of particles in a shear flow, *J. Colloid Interface Sci.* 187 (1997) 466–473, <https://doi.org/10.1006/jcis.1996.4710>.
- [9] G. Frappier, B.S. Lartiges, S. Skali-Lami, Floc cohesive force in reversible aggregation: a couette laminar flow investigation, *Langmuir* 26 (13) (2010) 10475–10488, <https://doi.org/10.1021/la9046947> ISSN 0743-7463.
- [10] P.T. Spicer, S.E. Pratsinis, Shear-induced flocculation: the evolution of floc structure and the shape of the size distribution at steady state, *Water Res.* 30 (5) (1996) 1049–1056, [https://doi.org/10.1016/0043-1354\(95\)00253-7](https://doi.org/10.1016/0043-1354(95)00253-7) ISSN 0043-1354.
- [11] D. Bouyer, R. Escudé, A. Liné, Experimental analysis of hydrodynamics in a jar-test, *Process Saf. Environ. Prot.* 83 (1) (2005) 22–30, <https://doi.org/10.1205/psep.03109> ISSN 0957-5820.
- [12] C. Coufort, D. Bouyer, A. Liné, Flocculation related to local hydrodynamics in a Taylor-Couette reactor and in a jar, *Chem. Eng. Sci.* 60 (8–9) (2005) 2179–2192, <https://doi.org/10.1016/j.ces.2004.10.038> ISSN 0009-2509.
- [13] L. Ehrl, M. Soos, M. Morbidelli, Dependence of aggregate strength, structure, and light scattering properties on primary particle size under turbulent conditions in stirred tank, *Langmuir* 24 (7) (2008) 3070–3081, <https://doi.org/10.1021/la7032302> ISSN 0743-7463.
- [14] M. Vlieghe, C. Coufort-Saudejaud, C. Frances, A. Liné, In situ characterization of floc morphology by image analysis in a turbulent Taylor-Couette reactor, *AIChE J.* 60 (7) (2014) 2389–2403, <https://doi.org/10.1002/aic.14431> ISSN 1547-5905.
- [15] T. Li, Z. Zhu, D. Wang, C. Yao, H. Tang, Characterization of floc size, strength and structure under various coagulation mechanisms, *Powder Technol.* 168 (2) (2006) 104–110, <https://doi.org/10.1016/j.powtec.2006.07.003> ISSN 0032-5910.
- [16] A. Vahedi, B. Górczyca, Predicting the settling velocity of flocs formed in water treatment using multiple fractal dimensions, *Water Res.* 46 (2012) 4188–4194, <https://doi.org/10.1016/j.watres.2012.04.031>.
- [17] R.K. Chakraborti, K.H. Gardner, J.F. Atkinson, J.E. Van Benschoten, Changes in fractal dimension during aggregation, *Water Res.* 37 (2003) 873–883, [https://doi.org/10.1016/S0043-1354\(02\)00379-2](https://doi.org/10.1016/S0043-1354(02)00379-2) ISSN 0043-1354.
- [18] T. Li, Z. Zhu, D. Wang, C. Yao, H. Tang, The strength and fractal dimension characteristics of alum-kaolin flocs, *Int. J. Miner. Proc.* 82 (1) (2007) 23–29, <https://doi.org/10.1016/j.minpro.2006.09.012> ISSN 0301-7516.
- [19] R.C. Sonntag, W.B. Russel, Structure and breakup of flocs subjected to fluid stresses. I. Shear experiments, *J. Colloid Interface Sci.* 113 (2) (1986) 399–413.
- [20] P.T. Spicer, S.E. Pratsinis, J. Raper, R. Amal, G. Bushell, G. Meesters, Effect of shear schedule on particle size, density, and structure during flocculation in stirred tanks, *Powder Technol.* 97 (1) (1998) 26–34, [https://doi.org/10.1016/S0032-5910\(97\)03389-5](https://doi.org/10.1016/S0032-5910(97)03389-5) ISSN 0032-5910.
- [21] R.B. Moruzzi, A.L. de Oliveira, F.T. da Conceição, J. Gregory, L.C. Campos, Fractal dimension of large aggregates under different flocculation conditions, *Sci. Total Environ.* 609 (2017) 807–814, <https://doi.org/10.1016/j.scitotenv.2017.07.194>.
- [22] P. Bubakova, M. Pivokonsky, P. Filip, Effect of shear rate on aggregate size and structure in the process of aggregation and at steady state, *Powder Technol.* 235 (2013) 540–549, <https://doi.org/10.1016/j.powtec.2012.11.014> ISSN 0032-5910.
- [23] K.A. Kusters, J.G. Wijers, D. Thoenes, Aggregation kinetics of small particles in agitated vessels, *Chem. Eng. Sci.* 52 (1997) 107–121, [https://doi.org/10.1016/S0009-2509\(96\)00375-2](https://doi.org/10.1016/S0009-2509(96)00375-2).
- [24] E. Barbot, P. Dussouillez, J.-Y. Bottero, P. Moulin, Coagulation of bentonite suspension by polyelectrolytes or ferric chloride: floc breakage and reformation, *Chem. Eng. J.* 156 (1) (2010) 83–91, <https://doi.org/10.1016/j.cej.2009.10.001> ISSN 1385-8947.
- [25] D. Bouyer, C. Coufort, A. Liné, Z. Do-Quang, Experimental analysis of floc size distributions in a 1-l jar under different hydrodynamics and physicochemical conditions, *J. Colloid Interface Sci.* 292 (2) (2005) 413–428, <https://doi.org/10.1016/j.jcis.2005.06.011> ISSN 0021-9797.
- [26] C. Coufort, C. Dumas, D. Bouyer, A. Liné, Analysis of floc size distributions in a mixing tank, *Chem. Eng. Process.* 47 (3) (2008) 287–294, <https://doi.org/10.1016/j.ccep.2007.01.009> ISSN 0255-2701.
- [27] F. Xiao, K.M. Lam, X.Y. Li, R.S. Zhong, X.H. Zhang, PIV characterization of flocculation dynamics and floc structure in water treatment, *Colloids Surf. A Physicochem. Eng. Aspects* 379 (1–3) (2011) 27–35, <https://doi.org/10.1016/j.colsurfa.2010.11.053> ISSN 0927-7757.
- [28] M.A. Yukselen, J. Gregory, The reversibility of floc breakage, *Int. J. Miner. Process.* 73 (2010) 251–259, [https://doi.org/10.1016/S0301-7516\(03\)00077-2](https://doi.org/10.1016/S0301-7516(03)00077-2) ISSN 0301-7516.
- [29] D. Wang, R. Wu, Y. Jiang, C.W.K. Chow, Characterization of floc structure and strength: role of changing shear rates under various coagulation mechanisms, *Colloids Surf. A Physicochem. Eng. Aspects* 379 (2011) 36–42, <https://doi.org/10.1016/j.colsurfa.2010.11.048> ISSN 0927-7757.
- [30] J. Duan, J. Gregory, Coagulation by hydrolysing metal salts, *Adv. Colloid Interface Sci.* 100 (102) (2003) 475–502, [https://doi.org/10.1016/S0001-8686\(02\)00067-2](https://doi.org/10.1016/S0001-8686(02)00067-2) ISSN 0001-8686.
- [31] C. Wu, Y. Wang, B. Gao, Y. Zhao, Q. Yue, Coagulation performance and floc characteristics of aluminum sulfate using sodium alginate as coagulant aid for synthetic dyeing wastewater treatment, *Sep. Purif. Technol.* 95 (2012) 180–187, <https://doi.org/10.1016/j.seppur.2012.05.009>.
- [32] J. Gregory, S. Barany, Adsorption and flocculation by polymers and polymer mixtures, *Adv. Colloid Interface Sci.* 169 (2011) 1–12, <https://doi.org/10.1016/j.cis.2011.06.004>.
- [33] L. Guérin, C. Coufort-Saudejaud, A. Liné, C. Frances, Dynamics of aggregate size and shape properties under sequenced flocculation in a turbulent Taylor-Couette reactor, *J. Colloid Interface Sci.* 491 (2017) 167–178, <https://doi.org/10.1016/j.jcis.2016.12.042>.
- [34] C.M. Sorensen, Light scattering by fractal aggregates: a review, *Aerosol Sci. Technol.* 35 (2) (2001) 648–687, <https://doi.org/10.1080/02786820117868> ISSN 0278-6826.
- [35] B.E. Logan, K. Rabaey, Conversion of wastes into bioelectricity and chemicals by using microbial electrochemical technologies, *Science* 337 (2012) 686–690, <https://doi.org/10.1126/science.1217412>.
- [36] Y. Adachi, M.A.C. Stuart, R. Fokkink, Kinetics of turbulent coagulation studied by means of end-over-end rotation, *J. Colloid Interface Sci.* 165 (1994) 310–317, <https://doi.org/10.1006/jcis.1994.1234>.
- [37] M.M. Takayasu, F. Galembeck, Determination of the equivalent radii and fractal dimension of polystyrene aggregates from sedimentation coefficients, *J. Colloid Interface Sci.* 202 (1998) 84–88, <https://doi.org/10.1006/jcis.1998.5428> ISSN 0021-9797.
- [38] C. Selomulya, R. Amal, G. Bushell, T.D. Waite, Evidence of shear rate dependence on restructuring and breakup of latex aggregates, *J. Colloid Interface Sci.* 236 (1) (2001) 67–77, <https://doi.org/10.1006/jcis.2000.7372> ISSN 0021-9797.
- [39] M. Vlieghe, C. Coufort-Saudejaud, A. Liné, C. Frances, QMOM-based population balance model involving a fractal dimension for the flocculation of latex particles, *Chem. Eng. Sci.* 155 (2016) 65–82, <https://doi.org/10.1016/j.ces.2016.07.044>.
- [40] J. Gregory, The density of particle aggregates, *Water Sci. Technol.* 36 (1997) 1–13 doi: [S0273-1223\(97\)00452-6](https://doi.org/10.1016/S0273-1223(97)00452-6).

Glossary

- A: floc area [μm^2]
 D_f : 3D-fractal dimension [–]
 D_{pf} : morphological fractal dimension [–]
 G : shear rate [s^{-1}]
 HSR : high shear rate value [s^{-1}]
 L : characteristic size [μm]
 LSR : low shear rate value [s^{-1}]
 P : floc perimeter [μm]
 V : floc volume [μm^3]
 $X(4,3)$: volume moment mean size [μm]
 $\langle \eta \rangle$: Mean Kolmogorov microscale [μm]